Numerical solution of Rosseland model for transient thermal radiation in non-grey optically thick media using enriched basis functions

Mustapha Malek[1], Nouh Izem[1,*], M Shadi Mohamed[2], Mohammed Seaid[3,4], Mohamed Wakrim[1]

[1] *Laboratory of Engineering Sciences, Faculty of Science, Ibn Zohr University Agadir, Morocco*
[2] *School of Energy, Geoscience, Infrastructure and Society, Heriot-Watt University, Edinburgh EH14 4AS, UK*
[3] *Department of Engineering, Durham University, South Road, Durham DH1 3LE, UK*
[4] *International Water Research Institute, University Mohammed VI Polytechnic, Benguerir, Morocco*

Abstract

Heat radiation in optically thick non-grey media can be well approximated with the Rosseland model which is a class of nonlinear diffusion equations with convective boundary conditions. The optical spectrum is divided into a set of finite bands with constant absorption coefficients but with variable Planckian diffusion coefficients. This simplification reduces the computational costs significantly compared to solving a full radiative heat transfer model. Therefore, the model is very popular for industrial and engineering applications. However, the opaque nature of the media often results in thermal boundary layers that requires highly refined meshes, to be recovered numerically. Such meshes can significantly hinder the performance of numerical methods. In this work we explore for the first time using enriched basis functions for the model in order to avoid using refined meshes. In particular, we discuss the finite element method when using basis functions enriched with a combination of exponential and hyperbolic functions. We show that the enrichment can resolve thermal boundary layers on coarse meshes and with few elements. Comparisons to the standard finite element method for thermal radiation in non-grey optically thick media with multi-frequency bands show the efficiency of the approach. Although we mainly study the enriched basis functions in glass cooling applications but the substantial saving in the computational requirements makes the approach highly relevant to a large number of engineering applications that involve solving the Rosseland model.

Keywords. Finite element method; Partition of unity method; Radiative heat transfer; Rosseland model; Glass cooling; Thermal boundary layers

Nomenclature

h_c	convective heat coefficient, $(J.kg^{-1}K^{-1})$	ε	diffusion scaling
α	emissivity	$\mathbf{s}$	angular direction
ϱ	reflectivity	I	intensity, $(J.m^{-2}\mu m)$
κ	absorption coefficient, (m^{-1})	φ	mean intensity, $(J.m^{-2})$
σ	scattering coefficient, (m^{-1})	Θ	temperature, (K)
k_c	heat conduction coefficient, $(W.m^{-1}K^{-1})$	B	Planck function, $(W.m^{-2}\mu m^{-1})$
ν	frequency variable, (μm^{-1})	Θ_b	surround medium temperature, (K)

*Corresponding author: n.izem@uiz.ac.ma

Θ_0	initial temperature, (K)	$\mathbb{S}^2$	unit sphere
t	time, (s)	$\mathbf{n}$	surface normal
$\mathbf{x}$	spatial coordinate, (m)	$\mathbf{s}'$	specular reflective angular direction
Ω	spatial domain	n_{b}	refractive index of the surrounding medium
$\partial\Omega$	domain boundary	n_{m}	refractive index of the material

1 Introduction

Resolving heat transfer is a crucial step in modelling many engineering applications. Heat is transmitted through three interactive mechanisms namely conduction, convection and radiation. In a general case modelling heat transfer involves modelling these mechanisms as well as the interaction between them. Conduction and convection happen on a relatively long time scale and transfer heat within the proximity of the heat source compared to radiation which transfers heat at the speed of light and can affect objects far away from the source. The modelling may also involve nonlinearities, boundary layers and irregularities [3]. Therefore, resolving heat transfer can present a significant challenge in such cases for thermal design of solids thermal and cooling systems [29, 30] as well as for liquids [36–38]. In this paper we look into transient heat transfer in hot solids and applications with general geometries. Two dominant mechanisms are involved, namely, conduction and radiation. Modelling such a problem is often not possible with analytical solutions if complicated geometries are studied. Furthermore, numerical solutions involve solving theoretical models for the transient radiative heat transfer which is recognized as highly demanding computationally especially in multi-dimensions [2, 12, 44].

An approximation for the radiative transfer can be achieved with the spherical harmonic models also known as $\mathrm{P_N}$ approximations. However, these models may also lead to a large number of complicated equations which are coupled in a complex manner, see for example [8]. To reduce the computational costs several authors developed simplified models that are less demanding but sufficiently accurate for practical purposes [20]. Other methods used for solving the transient radiative heat transfer include the ray-tracing method which solves the transport equation along rays for a given temperature distribution [18, 46] and the discrete ordinates method which considers only a finite number of directions for the discretization of angle variables [2, 17]. Among these approximations the Rosseland model is widely considered as the simplest for transient radiative heat transfer [42]. It consists of replacing the integro-differential equations for radiative transfer with a single heat equation including nonlinear diffusion coefficients [4]. The Rosseland approximation is well established in the case of matter radiating in vacuum [42]. In the more complicated case of a prescribed incident radiation intensity, the Rosseland approximation is based on asymptotic analysis involving non-trivial boundary layers analysis, see for instance [2, 46]. This is often used in applications with optically thick media and can produce numerical solutions which have the same accuracy as those obtained using the full radiative heat transfer but with a significantly less computational effort.

The Rosseland model has been used for applications in glass cooling [21, 48], ceramic manufacturing [5], viscous electrically conducting incompressible flows [11] and convection-radiation heat transfer [27, 49] among others. However, it should be noted that a major difficulty with the Rosseland approximation is related to boundary conditions. Natural boundary conditions for transport equations and for diffusion equations are of a very different nature. For instance, Dirichlet boundary conditions are admissible for diffusion equations but not for transport equations. A typical instance of natural boundary condition for a transport equation consists of prescribing the density of particles entering the spatial domain where the equation is to be solved. Although the use of the Rosseland approximation simplifies the radiative transfer but the coupling with conduction as well as the formation of steep boundary layers can still be very challenging to recover with numerical methods. For example the Finite Element (FE) method, which is very flexible in dealing with complicated geometries, can become severely limited when recovering high gradient solutions on such boundary layers. This becomes more of an issue in the time domain where the solution needs to be evaluated continuously over a large number

of timesteps. Especially, in the nonlinear case where small inaccuracies can escalate quickly over time to destabilize the numerical solution and render the FE method impractical [32]. Other numerical methods also face the similar difficulties.

To deal with these difficulties it is possible to improve the approximation properties of a numerical method by including enrichment functions that have better approximation properties compared to the standard basis functions. Hence, instead of using general polynomials as an approximation basis for the finite element method one may use exponential functions to capture steep boundary layers. The enrichment technique was originally proposed in the partition of unity (PU) method [28], which was first used to enrich the FE [19] and then the boundary element [41] but for solving wave problems. Here, oscillatory functions are included in the basis functions to capture waves propagation on coarse meshes instead of fine ones without compromising on the accuracy. The PU method has been used to solve heat transfer in homogeneous media [25, 32], in heterogeneous materials for two-dimensional applications [26] and recently in functionally graded materials for three-dimensional problems [24]. A major advantage for the PU enrichment approach is related to the global nature of the enrichment functions. Hence, the continuity between the elements is smoothly ensured through the combination of the enrichment with the standard polynomial shape functions. However, it is also possible to use the enrichment with discontinuous formulations where the enforced continuity gives more flexibility in the enrichment functions choice. In [23] the authors use oscillatory functions to recover the solution of the Helmholtz equation within the ultra-weak variational formulation framework. The continuity is weakly enforced through the least squares approach. Another discontinuous approach can be found in [9] where the FE method is enriched with plane waves and the continuity is enforced by using Lagrange multipliers. Other discontinuous approaches are also available in the literature [13].

The enrichment approach was also applied to solve heat transfer problems which involves steep gradients. An early work on the partition of unity finite element (PUFE) solution of the convection-diffusion problem can be found in [35] where the convergence rate of the standard FE method is improved by including exponential functions similar to the exact solution. Later, transient geothermal problems are considered using time-dependent enrichments in [47]. The time dependence of the enrichment helped to maintain its approximation properties by updating it at each timestep. Another approach for multi-scale problems involves solving for a local domain to build a suitable enrichment that is then incorporated into the solution of a global domain [40]. The work was also extended to deal with transient heat transfer [39] and was implemented for parallel simulation [22]. A family of time-independent Gaussian functions were implemented for the solution of both linear transient diffusion problems that involve steep gradients [32] and nonlinear transient diffusion problems in heterogeneous materials [26]. This class of functions account for various temporal stages of the solution, which led to a significant improvement in the efficiency as the system matrix does not change in time. A similar approach was also adapted for radiative heat transfer in a grey material [33] and for glass cooling where multiple frequency bands have been studied [34]. Using mixed enrichments, it was also possible to develop a similar framework for solving heat transfer in heterogeneous media [7]. Again here discontinuous formulation were proposed for solving advection-diffusion problems with enrichment [1, 10, 15].

Numerical solution of the Rosseland approximation of transient thermal radiation in non-grey optically thick media often presents difficulties because of the presence of external and internal boundary layers. In this paper we investigate for the first time the finite element solution of the Rosseland model using the PU enriched basis functions. The novelty in the present approach lies on the ability of the PUFE method to accurately resolves the thermal features in the Rosseland model on coarse meshes without requiring special treatment of the optical spectrum or solving nonlinear systems of algebraic equations. The presented results shows that the enriched basis functions can significantly reduce the number of degrees of freedom needed for the FE when solving the Rosseland approximation with steep boundary layers. This can be a major advantage when modelling radiative heat transfer for industrial applications where steep boundary layers can pose a significant challenge in terms of required degrees of freedom. The rest of the paper is organized as follows. The governing equations for the transient thermal radiation in non-grey media are stated in section 2. In section 3, we formulate a linearly implicit scheme for the time integration and the variational formulation for the space discretization is established using the FE method with PU enriched basis functions. The numerical results for three test examples including glass cooling are presented in section 4. Finally, section 5 contains some concluding remarks.

2 Equations for thermal radiation in non-grey media

In general, modelling thermal radiation in non-grey media requires integro-differential equations that depend on the space, direction and frequency due to the energy transport by photons, see for example [16, 20, 30]. The model consists of a heat equation for the temperature $\Theta(\mathbf{x}, t)$ and a transport equation for the radiative intensity $I(\mathbf{x}, \nu, \mathbf{s})$. These equations are given in a dimensionless form by

$$\begin{aligned}
\varepsilon^2 \frac{\partial \Theta}{\partial t} - \varepsilon^2 \nabla \cdot (k_c \nabla \Theta) &= -\int_{\nu_0}^{\infty} \kappa(\nu) \left(4\pi B(\Theta, \nu, n_{\mathrm{m}}) - \int_{\mathbb{S}^2} I(\mathbf{x}, \mathbf{s}, \nu) d\mathbf{s} \right) d\nu, \quad (\mathbf{x}, t) \in \Omega \times [0, T], \\
\varepsilon \mathbf{s} \cdot \nabla I + \kappa(\nu) I &= \kappa(\nu) B(\Theta, \nu, n_{\mathrm{m}}), \qquad (\mathbf{x}, \nu, \mathbf{s}) \in \Omega \times [\nu_0, \infty[\times \mathbb{S}^2, \\
\varepsilon k_c \mathbf{n}(\hat{\mathbf{x}}) \cdot \nabla \Theta + h_c(\Theta - \Theta_b) &= \alpha\pi \int_0^{\nu_0} \Big(B(\Theta_b, \nu, n_{\mathrm{b}}) - B(\Theta, \nu, n_{\mathrm{b}}) \Big) d\nu, \qquad (\hat{\mathbf{x}}, t) \in \partial\Omega \times [0, T], \qquad (1) \\
I(\hat{\mathbf{x}}, \mathbf{s}, \nu) &= \varrho(\mathbf{n} \cdot \mathbf{s}) I(\hat{\mathbf{x}}, \mathbf{s}', \nu) + \Big(1 - \varrho(\mathbf{n} \cdot \mathbf{s}) \Big) B(\Theta_b, \nu, n_{\mathrm{m}}), \quad (\hat{\mathbf{x}}, \nu, \mathbf{s}) \in \partial\Omega^- \times [0, \nu_0[\times \mathbb{S}^2, \\
\Theta(\mathbf{x}, 0) &= \Theta_0(\mathbf{x}), \qquad \mathbf{x} \in \Omega,
\end{aligned}$$

where Ω is a geometrical domain with a boundary $\partial\Omega$ of an absorbing and emitting semi-transparent material, $I(\mathbf{x}, \mathbf{s}, \nu)$ is the spectral intensity at the point $\mathbf{x}$ and the frequency ν, and with the propagation direction $\mathbf{s}$. The problem is considered in the time span $[0, T]$. Here, k_c is the thermal conductivity, κ the absorption coefficient, h_c the convective heat transfer coefficient, Θ_0 a given initial temperature of the media, Θ_b a given ambient temperature of the surrounding, $\mathbb{S}^2$ denotes the unit sphere, $\mathbf{n}(\hat{\mathbf{x}})$ the outward normal at $\hat{\mathbf{x}}$ to the boundary $\partial\Omega$, α the mean hemispheric surface emissivity in the opaque spectral region $[0, \nu_0]$ where radiation is completely absorbed, $\varepsilon \in (0, 1]$ is a diffusion scale, $\varrho \in [0, 1]$ is the reflectivity, and n_{b} and n_{m} are, respectively, the refractive indices of the surrounding medium and the semi-transparent material. In (1), $B(\Theta, \nu, n)$ is the spectral intensity of the black-body radiation defined by the Planck function in a medium with refractive index n as

$$B(\Theta, \nu, n) = \frac{2 h_P \nu^3}{c_0^2} n^2 \frac{1}{\exp\left(\dfrac{h_P \nu}{\kappa_B \Theta} \right) - 1}, \qquad (2)$$

where h_P is Planck's constant, κ_B Boltzmann's constant, and c_0 the speed of radiation propagation in the vacuum, see for instance [29]. Note that on the boundary we consider the transmitting and specular reflecting conditions where the boundary region $\partial\Omega^-$ in (1) is defined as

$$\partial\Omega^- = \Big\{ \hat{\mathbf{x}} \in \partial\Omega : \quad \mathbf{n}(\hat{\mathbf{x}}) \cdot \mathbf{s} < 0 \Big\},$$

and $\mathbf{s}' = \mathbf{s} - 2(\mathbf{n} \cdot \mathbf{s})\mathbf{n}$ is the specular reflection of $\mathbf{s}$ on $\partial\Omega$. In (1), the reflectivity ϱ is obtained according to the Fresnel and Snell laws. Thus, for an incident angle β_{m} given by $\cos\beta_{\mathrm{m}} = |\mathbf{n} \cdot \mathbf{s}|$ and the Snell law $n_{\mathrm{b}} \sin\beta_{\mathrm{b}} = n_{\mathrm{m}} \sin\beta_{\mathrm{m}}$, the reflectivity $\varrho(\mu)$, $\mu = |\mathbf{n} \cdot \mathbf{s}|$, is defined by

$$\varrho(\mu) = \begin{cases} \dfrac{1}{2} \left(\dfrac{\tan^2(\beta_{\mathrm{m}} - \beta_{\mathrm{b}})}{\tan^2(\beta_{\mathrm{m}} + \beta_{\mathrm{b}})} + \dfrac{\sin^2(\beta_{\mathrm{m}} - \beta_{\mathrm{b}})}{\sin^2(\beta_{\mathrm{m}} + \beta_{\mathrm{b}})} \right), & \text{if} \quad |\sin\beta_{\mathrm{m}}| \le \dfrac{n_{\mathrm{b}}}{n_{\mathrm{m}}}, \\ 1, & \text{otherwise.} \end{cases}$$

We assume that $n_{\mathrm{m}} > n_{\mathrm{b}}$ and the hemispheric emissivity α is related to the reflectivity ϱ by

$$\alpha = 2 n_{\mathrm{m}} \int_0^1 \Big(1 - \varrho(\mu) \Big) d\mu.$$

Details on the passage from dimensional equations to the dimensionless system (1) can be found in [16, 20] and are omitted here.

In the present study, we are interested in thermal radiation in non-grey optically thick media. For a semi-transparent medium with large scattering, an asymptotic expansion (for $\varepsilon \ll 1$) in (1) yields the equilibrium diffusion or the Rosseland approximation [2, 42, 46]

$$\begin{aligned}
\frac{\partial \Theta}{\partial t} - \nabla \cdot \Big(\Big(k_c + k_r\left(\Theta\right) \Big) \nabla \Theta \Big) &= 0, && (\mathbf{x}, t) \in \Omega \times [0, T] \\
\varepsilon k_c \mathbf{n}(\hat{\mathbf{x}}) \cdot \nabla \Theta + h_c(\Theta - \Theta_b) &= \alpha\pi \int_0^{\nu_0} \Big(B(\Theta_b, \nu, n_{\mathrm{b}}) - B(\Theta, \nu, n_{\mathrm{b}}) \Big) d\nu, && (\hat{\mathbf{x}}, t) \in \partial\Omega \times [0, T] \qquad (3) \\
\Theta(\mathbf{x}, 0) &= \Theta_0(\mathbf{x}), && \mathbf{x} \in \Omega,
\end{aligned}$$

where the conduction coefficient $k_r\left(\Theta\right)$ is defined as a function of the temperature by

$$k_r\left(\Theta\right) = \frac{4\pi}{3} \int_{\nu_0}^{\infty} \frac{1}{\kappa\left(\nu\right)} \frac{\partial B}{\partial \Theta}(\Theta, \nu, n_{\mathrm{m}}) d\nu. \qquad (4)$$

Following ideas reported in [16, 20, 45], the radiative spectrum $[\nu_0, \infty)$ is divided into a finite set of small intervals $[\nu_{k-1}, \nu_k)$ and we assume that the spectral absorption coefficients $\kappa(\nu)$ are piecewise constants with respect to the frequency ν *i.e.*,

$$\kappa(\nu) = \kappa_k, \qquad \forall\ \nu \in [\nu_{k-1}, \nu_k), \quad k = 1, 2, \ldots, M, \qquad (5)$$

with κ_k is constant and M is the total number of spectral bands. If we introduce the Planck function $B^{(k)}$ in the kth spectral band

$$B^{(k)}(\Theta, n) = \int_{\nu_{k-1}}^{\nu_k} B(\Theta, \nu, n) d\nu, \qquad k = 1, 2, \ldots, M,$$

then the Rosseland approximation (3) transforms to

$$\begin{aligned}
\frac{\partial \Theta}{\partial t} - \nabla \cdot \Big(K\left(\Theta\right) \nabla \Theta \Big) &= 0, \\
\varepsilon k_c \mathbf{n}(\hat{\mathbf{x}}) \cdot \nabla \Theta + h_c(\Theta - \Theta_b) &= \alpha\pi \Big(B^{(0)}(\Theta_b, n_{\mathrm{b}}) - B^{(0)}(\Theta, n_{\mathrm{b}}) \Big), \qquad (6) \\
\Theta(\mathbf{x}, 0) &= \Theta_0(\mathbf{x}),
\end{aligned}$$

where

$$K\left(\Theta\right) = k_c + \frac{4\pi}{3} \sum_{k=1}^{M} \frac{1}{\kappa_k} \frac{\partial B^{(k)}}{\partial \Theta}(\Theta, n_{\mathrm{m}}).$$

The Rosseland equations (6) are widely accepted as an accurate model for radiation transport in both participating and non-participating optically thick media. These equations do not have analytical solutions for general geometries and their numerical solutions lead to computationally demanding problems for nonlinear diffusion and when thermal boundary layers are present. To deal with these we investigate a PU enriched basis functions for the finite element solution of the problem.

3 Enriched basis function for the finite element method

The standard finite element method usually relies on linear or quadratic basis functions over many elements to approximate steep boundary layers. This results in highly refined meshes which become a huge computational burden especially in transient problems. Taking into account that the Rosseland model may require the simulation of lengthy transient phases before a steady state solution is reached, the inefficiency in the standard finite element method becomes clear. On the other hand, to avoid intensive computations the efficiency of the

method can be improved by enriching the basis functions. The enrichment functions can be chosen to reproduce the physical behaviour of the solution. Hence, functions with steep gradients can be used to reproduce steep boundary layers [33]. In the context of partition of unity methods, the terminology enrichment is only used to refer to the special functions that have certain advantageous properties hence, can improve the finite element approximation for the problem under study. Previous results show that enriched finite elements are significantly more efficient in capturing such layers even on coarse meshes [32–34]. Discontinuous enrichment methods using Lagrange multipliers to ensure inter-element continuity have also been investigated in [9, 13] among others. In the present work, the continuity is ensured in a natural form through multiplying the enrichment with the polynomial shape functions. It should be stressed that enriched finite element methods can also handle curved edges as well as the straight ones without much differences. For example, the partition of unity method has recently been used in [6] to enrich the iso-geometric analysis approach for which complex real-life geometries are represented exactly.

In this work the enrichment is built into the FE approximation space using the PU method [28]. It should be noted that other enrichment approaches are expected to lead to similar results. To solve the Rosseland approximation (6) with the FE method we first integrate in time. The time domain is divided into N_T equal intervals, *i.e.* timesteps, $[t_n, t_{n+1}]$ each of the duration $\Delta t = t_{n+1} - t_n$ where $n = 0, 1, \ldots, N_T$. Then we use a linearly semi-implicit scheme to write

$$\begin{aligned} \frac{\Theta^{n+1} - \Theta^n}{\Delta t} - \nabla \cdot \Big(K\left(\Theta^n\right) \nabla \Theta^{n+1} \Big) &= 0, \\ \varepsilon k_c \mathbf{n}(\hat{\mathbf{x}}) \cdot \nabla \Theta^{n+1} + h_c(\Theta^{n+1} - \Theta_b) &= \alpha\pi \Big(B^{(0)}(\Theta_b, n_\mathrm{b}) - B^{(0)}(\Theta^n, n_\mathrm{b}) \Big), \end{aligned} \tag{7}$$

where the notation Θ^n and Θ^{n+1} denotes the value of the temperature Θ at times t_n and t_{n+1}, respectively. Note that all nonlinear terms in (6) are explicitly evaluated at time t_n such that only linear systems of algebraic equations are needed to be solved for updating the temperature at time t_{n+1}. As in most finite element methods, the weak form of the boundary value problem (7) is obtained by multiplying with a set of test functions ϕ, integrating over the domain Ω, applying the divergence theorem and substituting the boundary conditions

$$\begin{aligned} \int_\Omega \frac{\Theta^{n+1} - \Theta^n}{\Delta t} \phi \, d\Omega + \int_\Omega K\left(\Theta^n\right) \nabla \Theta^{n+1} \cdot \nabla \phi \, d\Omega &= \oint_\Gamma \frac{h_c}{\varepsilon k_c} K\left(\Theta^n\right) \left(\Theta_b - \Theta^{n+1}\right) \phi \, d\Gamma + \\ & \oint_\Gamma \frac{\alpha\pi}{\varepsilon k_c} K\left(\Theta^n\right) \Big(B^{(0)}(\Theta_b, n_\mathrm{b}) - B^{(0)}(\Theta^n, n_\mathrm{b}) \Big) \phi \, d\Gamma, \end{aligned} \tag{8}$$

where $\phi \in H^1(\Omega)$ with $H^1(\Omega)$ being the well-known Sobolev space. To solve the weak form (8) with the standard finite element method, the domain Ω is meshed into a set of elements where the temperature is approximated in terms of the nodal values $C_j(t)$ and polynomial basis functions $N_j(\mathbf{x})$

$$\Theta_h(\mathbf{x}, t) = \sum_{j=1}^{N_d} C_j(t) N_j(\mathbf{x}), \tag{9}$$

where N_d is the number of mesh nodes. Using the PUFE method these nodal values C_j are expanded as a product of the polynomial functions $N_j(\mathbf{x})$ and Q enrichment functions $G_q(\mathbf{x})$ such that

$$\Theta_h(\mathbf{x}, t) = \sum_{j=1}^{N_d} \sum_{q=1}^{Q} C_{j,q}(t) N_j(\mathbf{x}) G_q(\mathbf{x}), \tag{10}$$

where $C_{j,q}$ is the degree of freedom corresponding to the product $N_j(\mathbf{x})G_q(\mathbf{x})$.

Two types of enrichment functions are considered in this study. First, a sum of hyperbolic tangent functions that are placed on the domain boundary

$$G_q(\mathbf{x}) = \sum_{e=1}^{N_e} \overline{G}_{q,e}(\mathbf{x}), \qquad\qquad q = 1, 2, \ldots, Q_1, \tag{11}$$

where we assume that the boundary is composed of N_e edges. A hyperbolic function $\overline{G}_{q,e}$ is defined on each edge as

$$\overline{G}_{q,e}(\mathbf{x}) = 1 + \tanh\left(\frac{\mathbf{x} - \mathbf{x}_e}{h_q}\right), \qquad e = 1, 2, \ldots, N_e, \tag{12}$$

with $\mathbf{x}_e$ being a given distance from the edge and h_q a parameter to control the steepness of the enrichment. The second type of enrichments is a set of Gaussian functions centred at $\mathbf{x}_c = (x_c, y_c)^\top$

$$G_q(\mathbf{x}) = \frac{\exp\left(-\left(\frac{\overline{r}}{\gamma}\right)^{(q-Q_1)}\right) - \exp\left(-\left(\frac{\beta}{\gamma}\right)^{(q-Q_1)}\right)}{1 - \exp\left(-\left(\frac{\beta}{\gamma}\right)^{(q-Q_1)}\right)}, \qquad q = Q_1 + 1, Q_1 + 2, \ldots, Q, \tag{13}$$

where $\overline{r} = \|\mathbf{x} - \mathbf{x_c}\|$ is the distance between any given point $\mathbf{x}$ and the centre $\mathbf{x}_c$. Again here the parameters γ and β are parameters to control the steepness of the enrichment function G_q.

The finite element approximation space can then be defined as

$$\widetilde{V}_h = \text{span}\left\{ N_j(\mathbf{x})G_q(\mathbf{x}), \qquad \Theta_h(\mathbf{x}) = \sum_{j=1}^{N_d}\sum_{q=1}^{Q} C_{j,q} N_j(\mathbf{x})G_q(\mathbf{x}) \right\}.$$

The derivatives of the new shape function for $(1 \leq q \leq Q_1)$ are given by

$$\frac{\partial N_j(\mathbf{x})G_q(\mathbf{x})}{\partial x} = G_q(\mathbf{x})\frac{\partial N_j(\mathbf{x})}{\partial x} + \frac{1}{h_q}\left(1 - \tanh^2\left(\frac{x - x_e}{h_q}\right)\right) N_j(\mathbf{x}),$$

$$\frac{\partial N_j(\mathbf{x})G_q(\mathbf{x})}{\partial y} = G_q(\mathbf{x})\frac{\partial N_j(\mathbf{x})}{\partial y} + \frac{1}{h_q}\left(1 - \tanh^2\left(\frac{y - y_e}{h_q}\right)\right) N_j(\mathbf{x}).$$

and for $(Q_1 < q \leq Q)$ by

$$\frac{\partial N_j(\mathbf{x})G_q(\mathbf{x})}{\partial x} = G_q(\mathbf{x})\frac{\partial N_j(\mathbf{x})}{\partial x} - (q - Q_1)\frac{\exp\left(-\left(\frac{\overline{r}}{\gamma}\right)^{(q-Q_1)}\right)}{1 - \exp\left(-\left(\frac{\beta}{\gamma}\right)^{(q-Q_1)}\right)}\frac{\overline{r}^{(q-Q_1-2)}}{\gamma^{(q-Q_1)}}(x - x_0)N_j(\mathbf{x}),$$

$$\frac{\partial N_j(\mathbf{x})G_q(\mathbf{x})}{\partial y} = G_q(\mathbf{x})\frac{\partial N_j(\mathbf{x})}{\partial y} - (q - Q_1)\frac{\exp\left(-\left(\frac{\overline{r}}{\gamma}\right)^{(q-Q_1)}\right)}{1 - \exp\left(-\left(\frac{\beta}{\gamma}\right)^{(q-Q_1)}\right)}\frac{\overline{r}^{(q-Q_1-2)}}{\gamma^{(q-Q_1)}}(y - y_0)N_j(\mathbf{x}).$$

To have a better insight, Figure 1 shows plots of the shape functions resulting from combining the first three orders of the Gaussian enrichment functions with the three polynomial shape functions associated with the linear triangular elements. The row j in Figure 1 corresponds to the polynomial shape function $N_j(\mathbf{x})$ while the column q correspond to the enrichment $G_q(\mathbf{x})$. The intersection of each row and column shows the resulting shape function $N_j(\mathbf{x})G_q(\mathbf{x})$ that corresponds to that row and column. The plots are shown on a mesh composed of 32 uniform elements for simplicity in the presentation. For demonstration purposes the function $N_j(\mathbf{x})G_q(\mathbf{x})$ is plotted element-wise rather than over the patches associated with each node. Obviously, a node shared between some elements does not always correspond to the same N_j in all these elements. Figure 1 also shows

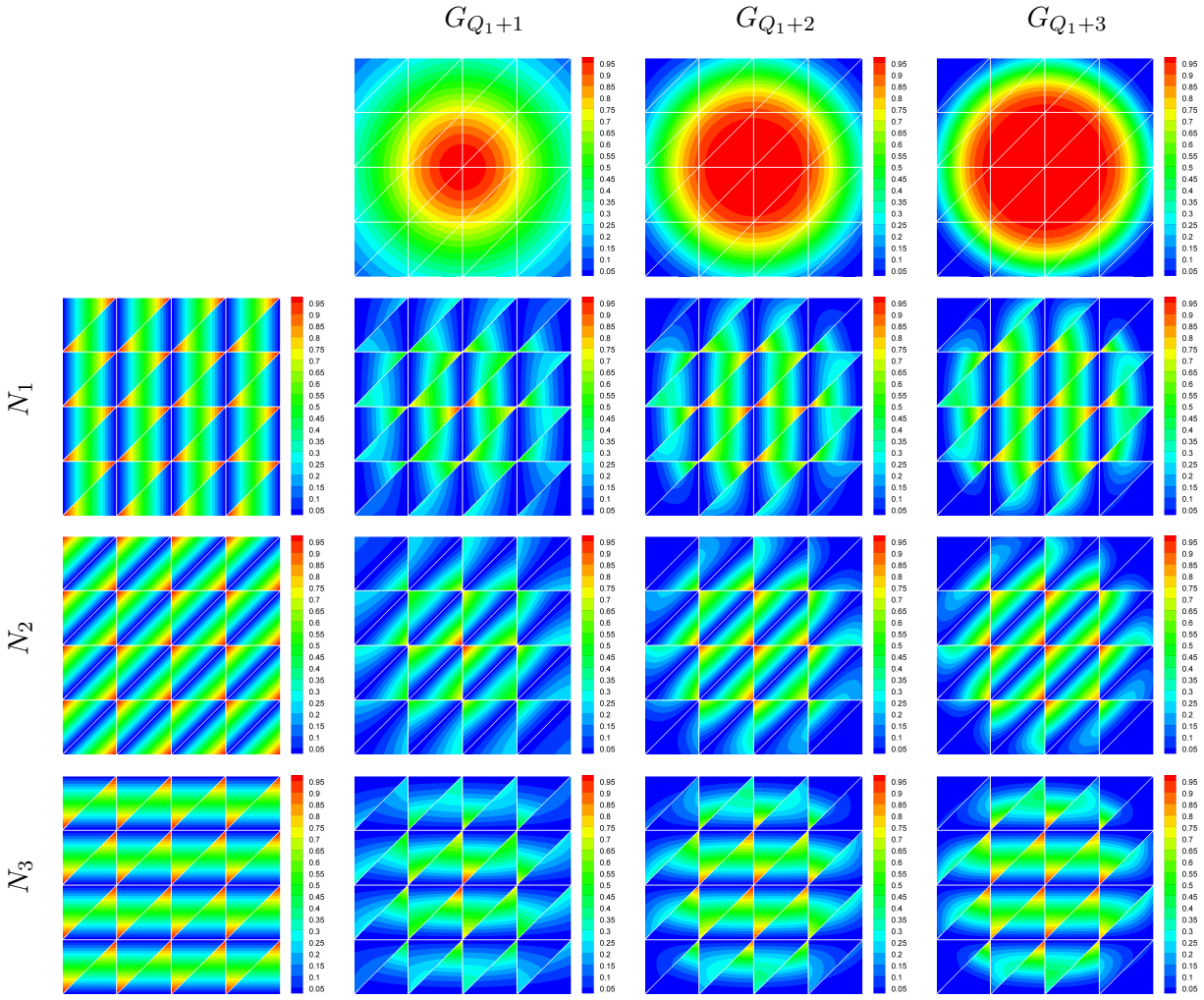

Figure 1: Polynomial shape functions $N_j(\mathbf{x})$ (first column), Gaussian enrichment functions $G_q(\mathbf{x})$ (first row) and the resulting shape function $N_j(\mathbf{x})G_q(\mathbf{x})$ from multiplying enrichment q with polynomial j at the intersection of the rows and columns.

that for the polynomial shape functions all the elements have exactly the same approximation properties. However, using the enrichment the approximation properties become different between elements which can be clearly seen in the figure. To evaluate the elementary matrices we use the standard Gauss quadrature. Obviously, evaluating the function $N_j(\mathbf{x})G_q(\mathbf{x})$ requires more integration points per element compared to evaluating the polynomial functions $N_j(\mathbf{x})$. However, in order to achieve similar accuracy the FE method requires a lot more elements, hence, in total more integration points compared to the PUFE method.

To solve the fully discretized problem, the elementary matrices are assembled into a global system of equations

$$\mathcal{A}\mathbf{v} = \mathbf{b}. \tag{14}$$

The dimensions of an elementary matrix is expanded by a factor of Q when the enriched basis are used. The linear system of equations resulting from the enrichment is also expanded by the same factor *i.e.* Q. Adding enrichment does not change the sparsity pattern of the matrix $\mathcal{A}$ but it increases both the non-zero as well as the zero entries by a factor of Q^2. Again the FE need a lot more degrees of freedom, hence, results into much

larger linear systems compared to the PUFE. It should be stressed that using the enrichment does not break the symmetry of the matrix $\mathcal{A}$ in (14). However, it is known that the enrichment affects the conditioning of $\mathcal{A}$ where increasing the number of enrichment functions often worsen the conditioning. This does not affect the accuracy of the computed solution when only fewer than 10 enrichment functions are used in the simulation, see for instance [33, 34]. Also previous numerical studies shows that iterative solvers can also be used to solve the system (14) despite the ill-conditioning issue [31]. In the present study, the matrix is decomposed into an $LUL^\top$ factorization, then the solution is reduced to backward/forward substitutions after updating the global matrix $\mathcal{A}$ and the right-hand side vector $\mathbf{b}$ at every timestep.

4 Numerical results and applications

This section is devoted to numerical results for thermal radiation in glass cooling applications. We examine the accuracy and the performance of the considered PUFE method in both grey and non-grey media. For a grey media the Planck function in (3) reduces to

$$B(\Theta) = a_R \Theta^4, \tag{15}$$

where $a_R = 5.67 \times 10^{-8}$ is the radiation constant [30]. Hence, the Rosseland approximation (3) becomes

$$\begin{aligned} \frac{\partial \Theta}{\partial t} - \nabla \cdot \Big(\kappa(\Theta) \nabla \Theta \Big) &= 0, \\ \varepsilon k_c \mathbf{n}(\hat{\mathbf{x}}).\nabla \Theta + h_c(\Theta - \Theta_b) &= \alpha \pi \left(a_r \Theta_b^4 - a_r \Theta^4 \right), \\ \Theta(\mathbf{x}, 0) &= \Theta_0(\mathbf{x}), \end{aligned} \tag{16}$$

where the nonlinear diffusion coefficient $\kappa(\Theta)$ is given by

$$\kappa(\Theta) = k_c + \frac{16\pi}{3} a_r \Theta^3. \tag{17}$$

The ambient temperature is $\Theta_b = 300$K and the initial temperature $\Theta_0 = 1000$K. In the case of non-grey media we consider test examples in glass cooling process. The presented simulations use data kindly provided by ITWM [14], where the non-opaque frequency spectrum $[\nu_0, \infty)$ is approximated by an eight-band model. Since the data are originally defined by wavelength intervals $[\lambda_{k-1}, \lambda_k]$ $(k = 1, 2, \ldots, 8)$, we compute the corresponding frequency bands using the relation

$$\nu_k = \frac{c_0}{\lambda_k \, n_m}.$$

The values used in this study for absorption coefficients for glass cooling are given in Table 1. Note that the glass is considered to be opaque to radiation for wavelengths larger than a cut-off wavelength equal to 6 μm.

Unless otherwise stated, the enrichment is defined by the following parameters. The hyperbolic enrichment is constructed with the edge parameters $\mathbf{x}_1 = (-0.01, 0)^\top, \mathbf{x}_2 = (0, -0.01)^\top, \mathbf{x}_3 = (1.01, 0)^\top$ and $\mathbf{x}_1 = (0, 1.01)^\top$, while the steepness parameters are $h_1 = 0.05, h_2 = 0.10, h_3 = 0.20$ and $h_4 = 5.00$. The Gaussian enrichment is centred at $\mathbf{x}_c = (0.50, 0.50)^\top$ with the following values for the steepness parameters $\gamma = \frac{8}{9}$ and $\beta = 8$. It should be stressed that comparisons between results obtained using the Rosseland and those obtained using the full radiative heat transfer model have been carried out in [16, 20] among others.

4.1 Accuracy test problem

In order to check the accuracy of the proposed PUFE method, we solve a modified Rosseland problem with a manufactured analytical solution that was first proposed in [43]. We replace the right-hand-side terms in the first and second equations in (16) by a source function $f(t, x, y)$ and a boundary function $g(t, x, y)$, respectively.

Table 1: The eight-band spectrum and their associated frequencies, wavelengths and absorption coefficients used in our simulations for glass cooling.

Band k	ν_{k-1} $[10^{13}\mathrm{s}^{-1}]$	ν_k $[10^{13}\mathrm{s}^{-1}]$	λ_k $[\mu\mathrm{m}]$	λ_{k-1} $[\mu\mathrm{m}]$	κ_k $[\mathrm{m}^{-1}]$
—	0	2.9334638	7.00	∞	Opaque
1	2.9334638	3.4223744	6.0	7.0	7136.00
2	3.4223744	3.7334994	5.5	6.0	576.32
3	3.7334994	4.5631659	4.5	5.5	276.98
4	4.5631659	5.1335616	4.0	4.5	27.98
5	5.1335616	5.8669276	3.5	4.0	15.45
6	5.8669276	6.8447489	3.0	3.5	7.70
7	6.8447488	102.6712329	0.2	3.0	0.50
8	102.6712329	∞	0.0	0.2	0.40

The initial condition Θ_0 and the functions $f(t,x,y)$ and $g(t,x,y)$ are chosen so that the analytical solution of this problem is

$$\overline{\Theta}(t,x,y) \quad = \quad \cos\left(\frac{\pi x}{4}\right)\cos\left(\frac{\pi y}{4}\right)e^{-k_c t}.$$

This problem is selected to provide a tool for evaluating the numerical solution errors by comparing them to the analytical solution. However, since the analytical solution does not represent a specific physical meaning we take only numerical values without considering any units here. The problem is solved in a squared domain $\Omega = [0,1]\times[0,1]$. The nonlinear diffusion coefficient is given by (17) with $k_c = 0.01$ and $h_c = 0.001$. To measure the difference between the analytical and the numerical solutions we consider the following relative error

$$\frac{\left\|\Theta - \overline{\Theta}\right\|_{L^2(\Omega)}}{\left\|\overline{\Theta}\right\|_{L^2(\Omega)}}, \tag{18}$$

where $\|\cdot\|_{L^2(\Omega)}$ is the L^2-norm, Θ and $\overline{\Theta}$ are respectively, the computed and the analytical solutions.

Our first aim in this test example is to quantify the errors in the proposed PUFE when refining the temporal discretizations. We consider $\Delta t = 0.1$ then we half it to $\Delta t = 0.5$ and again to $\Delta t = 0.25$. The three time steps are then used to solve the problem on two meshes and with three different numbers of enrichment functions. The considered meshes are composed of 128 or 512 uniform 3-noded elements. The meshes are referred to with the edge size *i.e.* $h = \frac{1}{8}$ and $h = \frac{1}{16}$. The considered numbers of enrichment functions are $Q = 4, 6$ and 8 with $Q_1 = 0$ in all cases where only Gaussian enrichment functions are considered for this part of the results. The errors obtained for different spatial and temporal discretization at the time instance $t = 3$ are displayed in Table 2. As it can be seen from the results, by fixing the number of enrichment and decreasing the timestep Δt the PUFE method exhibits a good convergence for both selected meshes. It is also evident that for a fixed mesh more accurate results can be achieved by increasing the number of enrichment. Similarly, for the same Q and the same timestep refining the mesh improves the error. This behaviour suggests that using enriched basis functions consistently leads to improved errors when refining the temporal discretization for the different resolutions considered in the spatial discretization. It is important to note that due to the semi-implicit nature of the time stepping scheme the timestep Δt is required to satisfy the stability condition due to the explicit treatment of the nonlinear term in the problem. This stability condition varies mainly based on the values

Table 2: Relative errors obtained for decreased timesteps Δt using the PUFE methods with different enrichment numbers and mesh grids at $t = 3$.

	$h = \frac{1}{8}$			$h = \frac{1}{16}$		
Δt	$Q = 4$	$Q = 6$	$Q = 8$	$Q = 4$	$Q = 6$	$Q = 8$
0.1	7.91E-03	1.91E-03	4.30E-04	2.52E-03	5.88E-04	1.28E-04
0.05	4.54E-03	1.06E-03	2.31E-04	1.42E-03	3.19E-04	6.62E-05
0.025	2.43E-03	5.48E-04	1.15E-04	7.44E-04	1.61E-04	3.20E-05

Table 3: Relative errors obtained for the accuracy test using the PUFE method with different enrichment numbers and different meshes at time $t = 3$ using $\Delta t = 0.1$.

	$\Delta t = 0.1$							
Q	$h = 1$	$h = \frac{1}{2}$	$h = \frac{1}{4}$	$h = \frac{1}{8}$	$h = \frac{1}{16}$	$h = \frac{1}{32}$	$h = \frac{1}{64}$	$h = \frac{1}{128}$
2	5.62E-01	2.28E-01	8.64E-02	3.06E-02	1.01E-02	3.10E-03	8.91E-04	2.39E-04
4	1.61E-01	6.33E-02	2.32E-02	7.91E-03	2.52E-03	7.49E-04	2.08E-04	5.38E-05
6	4.32E-02	1.64E-02	5.79E-03	1.91E-03	5.88E-04	1.69E-04	4.52E-05	1.13E-05
8	1.08E-02	3.95E-03	1.35E-03	4.30E-04	1.28E-04	3.55E-05	9.18E-06	2.22E-06

of the mesh parameter h, the values of the temperature as well as the number of enrichments used in the simulations.

Our next aim in this example is to confirm the convergence of the PUFE method with respect to the spatial discretization. We first mesh the domain into 2 uniform 3-noded elements. This mesh is identified by the edge length $h = 1$. We then half the edge length to create a second mesh, namely, $h = \frac{1}{2}$ composed of 8 uniform 3-noded elements. We repeat the same for creating the meshes $h = \frac{1}{4}$, $\frac{1}{8}$, $\frac{1}{16}$, $\frac{1}{32}$, $\frac{1}{64}$ and $\frac{1}{128}$. All the meshes are then considered with a further spatial discrimination in terms of increasing the number of enrichment functions. Again only Gaussian functions are considered with $Q_1 = 0$ and the enrichment numbers $Q = 2, 4, 6$ and 8. One timestep is considered, namely, $\Delta t = 0.1$. In Table 3 we summarize the results obtained for different spatial discretizations in terms of h and Q at the time instance $t = 3$. It is clear that refining the mesh or increasing the number of enrichments results in a decrease in the computed relative errors. A faster decay in these errors is also detected for increasing the number of enrichment rather than refining the mesh. However, as it can be clearly observed in Table 3, consistent convergence is obtained in both h and Q refinements. It should also be mentioned that for a fixed error in the considered problem one can always find the optimal pair (h,Q) leading to the desired accuracy. The advantage of PUFE method over the conventional FE method lies on the fact that the desired accuracy can be achieved by increasing the number of enrichments Q but without changing the original mesh.

4.2 Thermal radiation in squared enclosures

In this test example we again consider a conduction-radiation problem in the unit square $\Omega = [0, 1] \times [0, 1]$. Here we aim to verify the performance of the PUFE method compared to the conventional FE method in terms of the accuracy and the efficiency. To this end three meshes with different element densities are considered and displayed in Figure 2. The finest mesh is composed of 8815 nodes and referred to as Mesh 3 which is used to

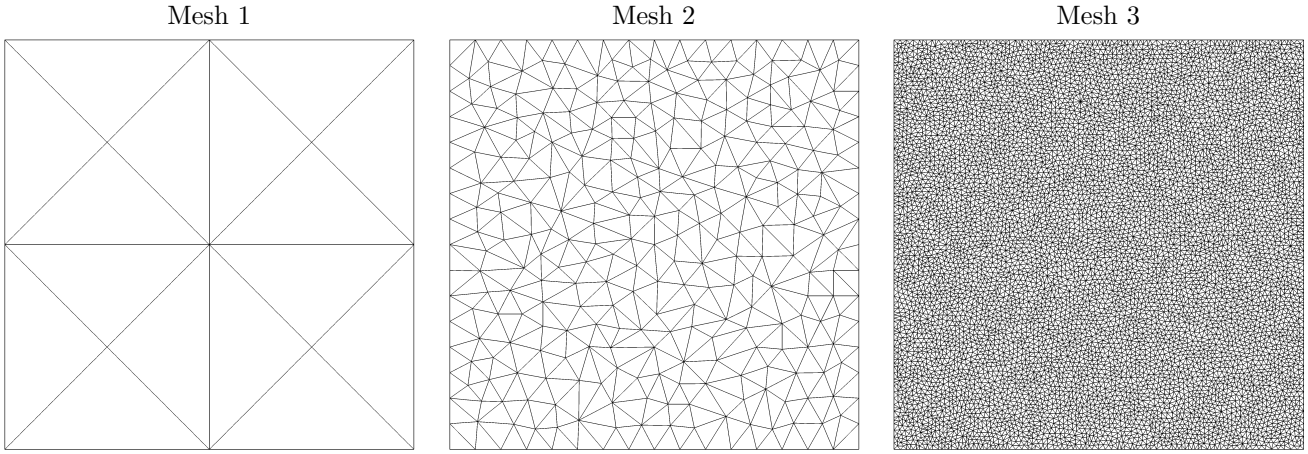

Figure 2: Meshes considered for the problem of thermal radiation in the squared enclosure. The number of elements and nodes is displayed under each mesh.

compute a reference solution with the FE method. The coarse mesh, namely, Mesh 1 is equipped with eight enrichment functions comprising four Gaussian and four hyperbolic functions. The total number of degrees of freedom for the PUFE solution on Mesh 1 is 104. The PUFE results are compared to the FE results obtained on Mesh 3 and on Mesh 2. The FE solution on Mesh 2 is obtained with 303 degrees of freedom which is higher than the number used with the PUFE solution. It should be noted that in industrial applications it is common to use adaptive mesh refinement for FE solution of this type of problems. This involves using fewer elements but also extra computations to evaluate the error as well as to generate mesh refinements. However, to present a clear and a direct comparison to the PUFE solution, we keep the FE mesh unchanged throughout the time domain. The simulations are performed with the timestep $\Delta t = 5 \times 10^{-5}$s.

In the case of a grey media, the Planck function is reduced to (15) and the problem to be solved is given by the equations (16)-(17). The results obtained using the PUFE method on Mesh 1 against the FE method on Mesh 2 and Mesh 3 are presented in Figure 3 for the optical regime $\varepsilon = 0.1$ and 1. Comparing the temperature distributions in the figure for both values of ε, fast cooling in the enclosure is observed for the larger value of the diffusion scale ε while steeper thermal boundary layers are observed for the smaller value of ε. As the time progresses the temperature reaches a steady state for both diffusion regimes. It is clear that the results presented in Figure 3 confirm that using Mesh 1 for the PUFE method yields the same temperature distributions as those obtained using the FE method on the fine mesh Mesh 3. It is also evident that for the considered radiative conditions, both the FE and the PUFE methods capture the temperature solutions and accurately resolve the moving thermal fronts in the enclosure. However, the FE results are computed on a fine mesh with 17251 elements and 8815 nodes while, the PUFE results are computed using a coarse mesh with 16 elements and 13 nodes and 8 enrichment functions which is a substantial reduction of the total number of degrees of freedom. Furthermore, the same simulations when using the FE method on the coarse mesh exhibits a noticeable degradation in the results where Figure 3 shows nonphysical oscillations in the solution. This failure to capture the correct temperature distribution is very clear in the FE results at early timesteps and specially for the case with $\varepsilon = 0.1$. On the other hand the PUFE method accurately resolves this test problem on a coarse mesh for the selected optical regimes. To illustrate the similarities between the solution obtained with the proposed PUFE method and the reference solution, we compare in Figure 4 the cross-section of the temperature along the horizontal centerline $y = 0.5$ for $\varepsilon = 0.1$ and $\varepsilon = 1$. It can be seen in the figure that the PUFE results are free from any nonphysical oscillations and coincide with the reference solutions.

Next, we consider the above test example but for a non-grey media where the Planck function is given by the expression (2) and the problem to be solved is given by (6). As in the previous simulations, we use the meshes

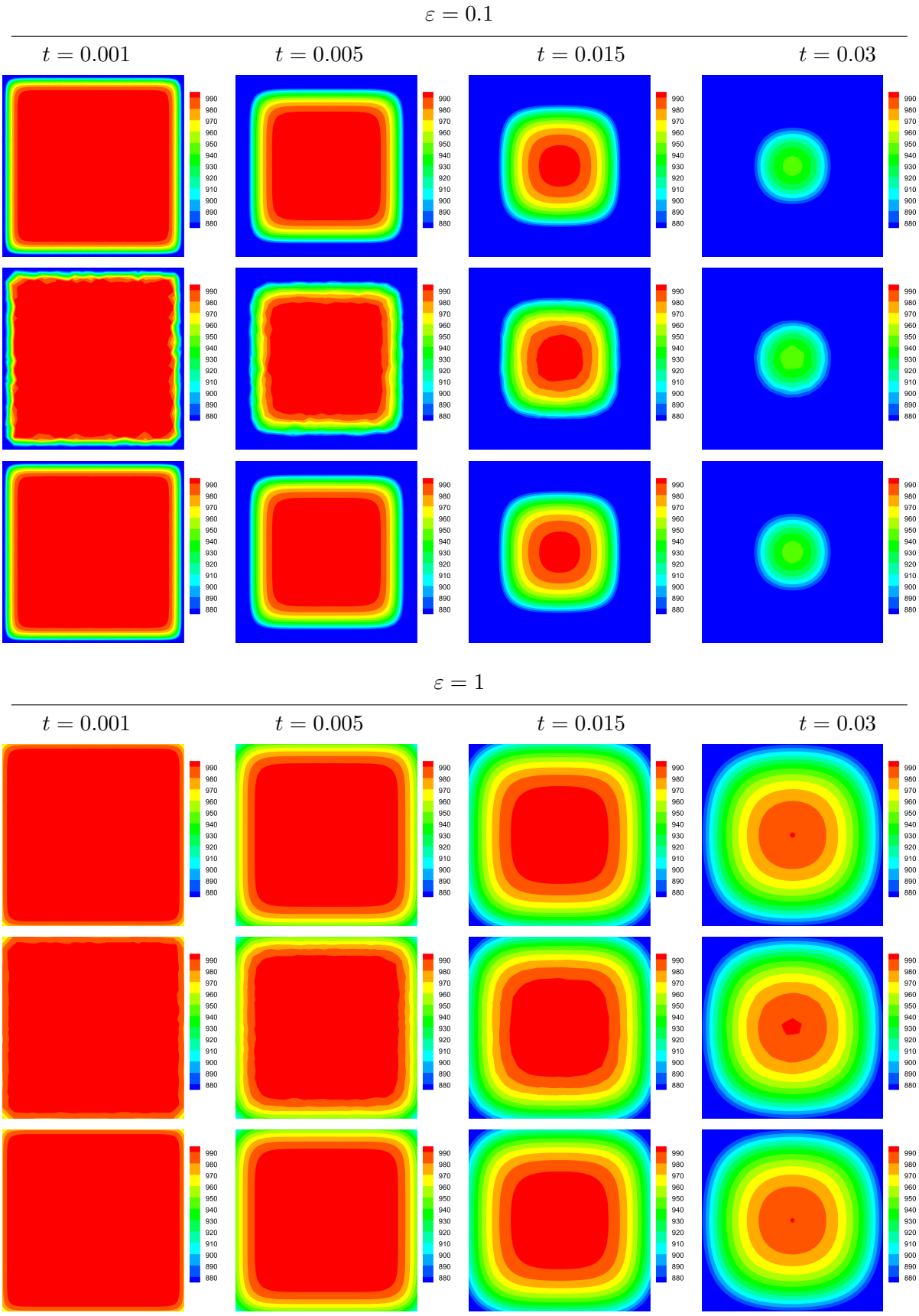

Figure 3: Temperature (K) distributions for the test example of the thermal radiation in a grey media. The results obtained using the FE method on Mesh 3 (first and fourth rows), the FE method on Mesh 2 (second and fifth rows) and the PUFE method on Mesh 1 (third and sixth rows). From left to right the simulation time is $t = 0.001$s, 0.005s, 0.015s and 0.03s.

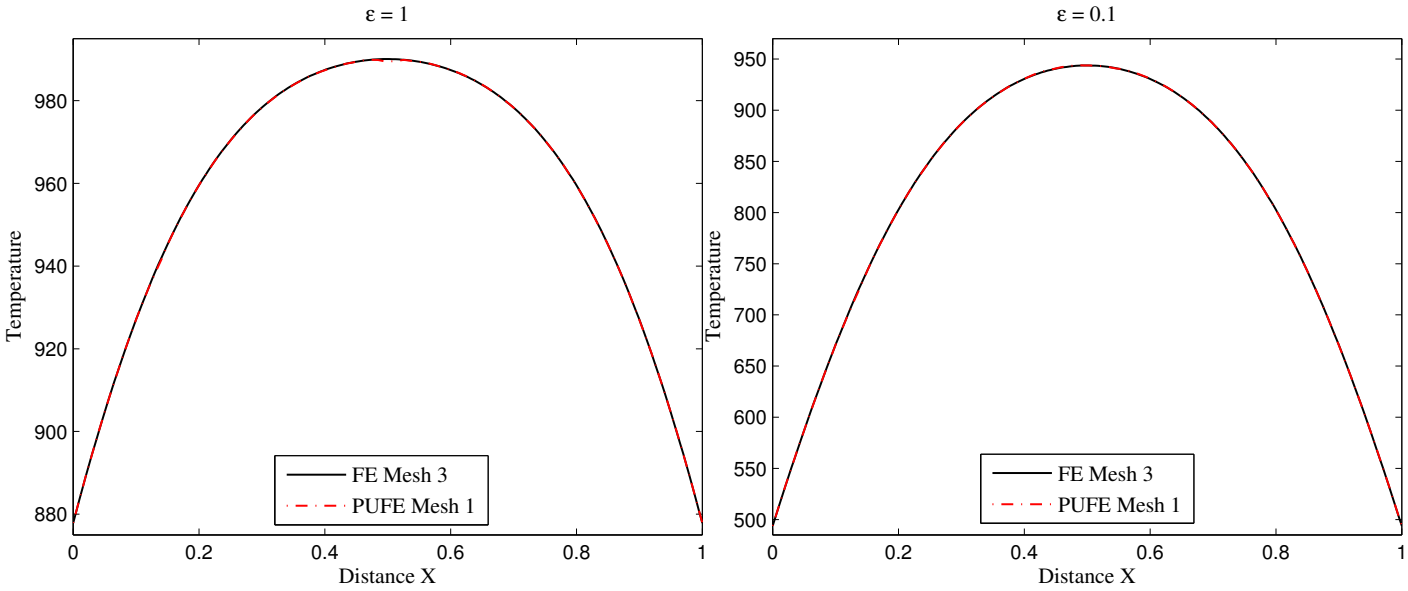

Figure 4: Cross-sections of the temperature (K) along the horizontal centerline for the test example of the thermal radiation in a grey media at time $t = 0.03$s for $\varepsilon = 1$ (left column) and $\varepsilon = 0.1$ (right column).

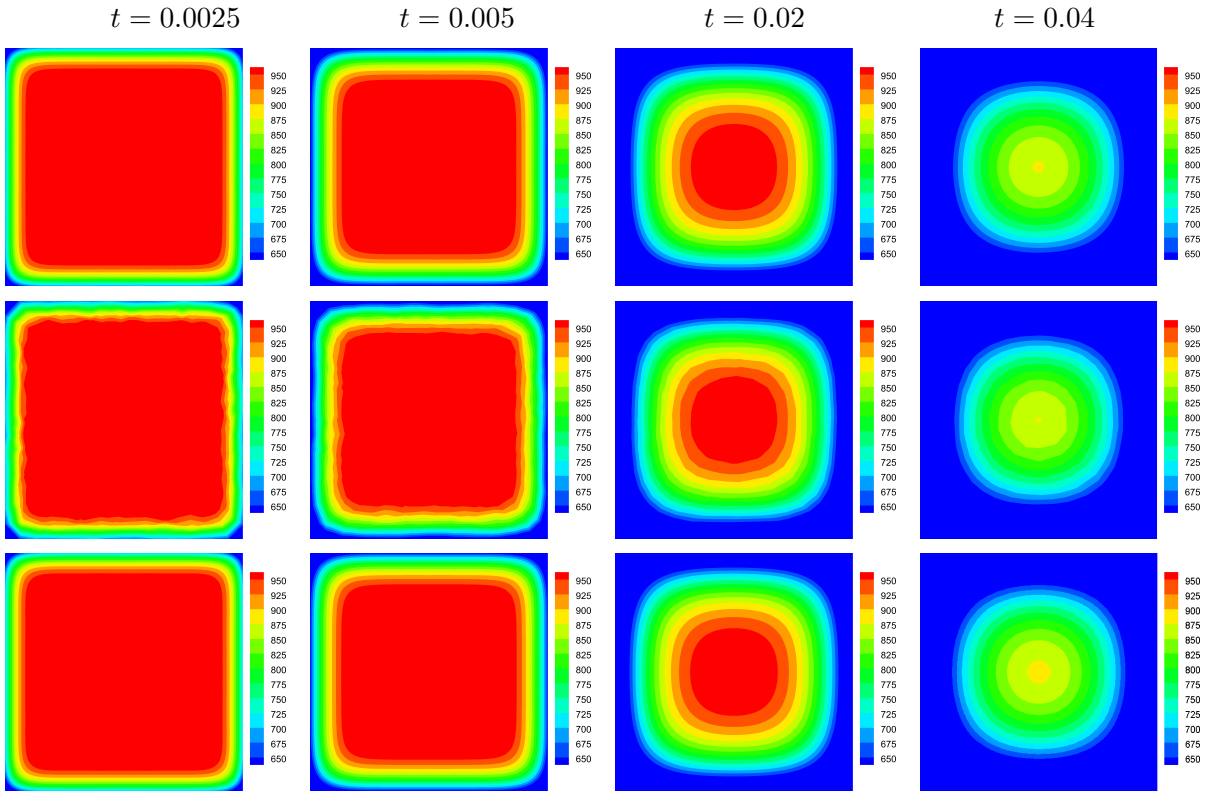

Figure 5: Temperature (K) distributions obtained using the FE method on Mesh 3 (first row), FE method on Mesh 2 (second row) and the PUFE method on Mesh 1 (third row) for the test example of the thermal radiation in a non-grey media. From left to right the simulation time $t = 0.0025$s, 0.005s, 0.02s and 0.04s.

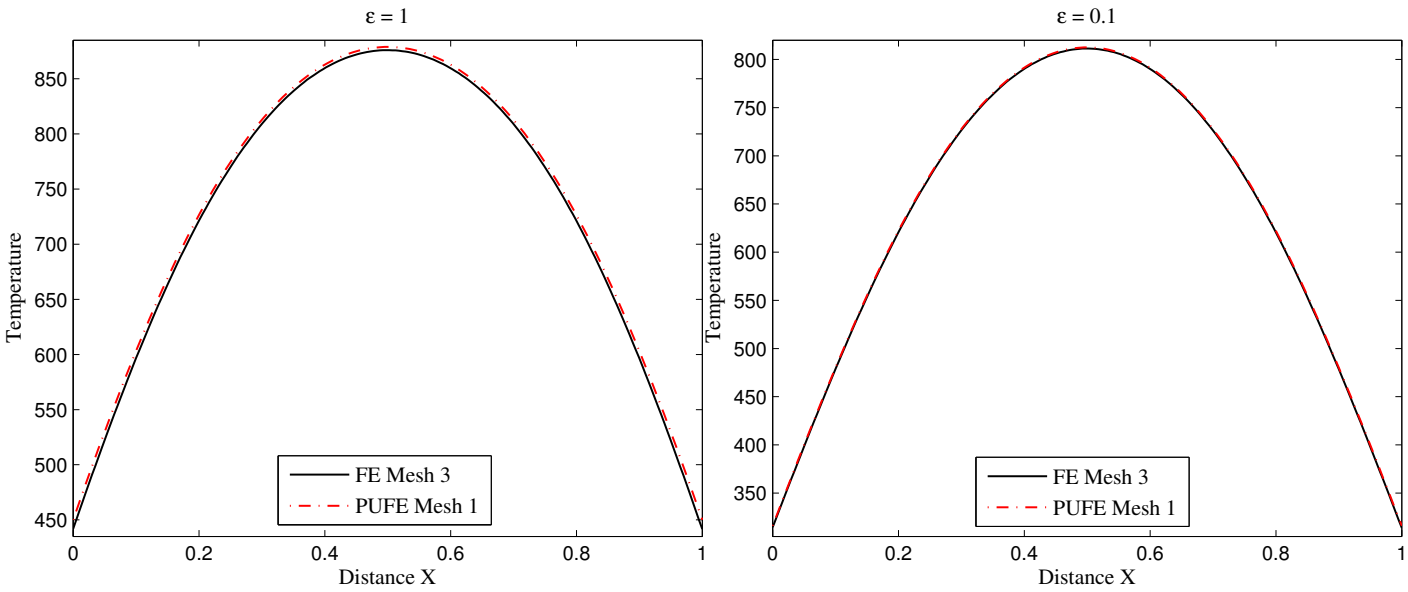

Figure 6: Cross-sections of the temperature (K) along the horizontal centerline for the test example of the thermal radiation in a non-grey media at time $t = 0.04$s for $\varepsilon = 1$ (left column) and $\varepsilon = 0.1$ (right column).

Table 4: Geometry and boundary temperature used for the test example of thermal radiation in circular inclusions shown on the domain in Figure 7.

	Γ_1	Γ_2	Γ_3	Γ_4
Center coordinates (m)	$(0.5, 0.5)$	$(0.5, 0.8)$	$(0.3, 0.4)$	$(0.7, 0.5)$
Radius (m)	0.5	0.08	0.12	0.10
Boundary temperature (K)	300	300	500	100

displayed in Figure 2 and the FE solution on the finest mesh Mesh 3 is considered as a reference solution. Again we use eight enrichment functions ($Q = 8$) with four Gaussian functions and four hyperbolic tangent functions. Figure 5 displays the temperature distributions for the diffusion scale $\varepsilon = 1$ obtained using the FE method on the coarse and fine meshes against the PUFE solution on Mesh 1. As in the previous case, for this non-grey media the PUFE method using few degrees of freedom is capable of recovering a temperature distribution very similar to the one obtained with the reference solution. For the considered optical spectrum the FE method on the coarse mesh also exhibits nonphysical oscillations in the temperature distribution which can be seen in Figure 5. Similar behaviour has been observed for the case with $\varepsilon = 0.1$ but the results are not reported here for brevity. Finally, to confirm the similarities between the PUFE and the reference solutions, Figure 6 displays the results obtained along the central cross-section at $y = 0.5$. It can clearly be seen in this figure that both solutions closely coincide. Therefore one may conclude that the PUFE method performs well for the Rosseland model on these enclosures and resolves all the thermal features without the need for refined meshes.

4.3 Thermal radiation in circular enclosures

For our final test example we resolve the thermal non-grey radiation in a circular domain with three holes where the problem geometry is illustrated in Figure 7. Here, we try to evaluate the performance of the PUFE method when the computational domain has a relatively complicated geometry and the mesh is unstructured.

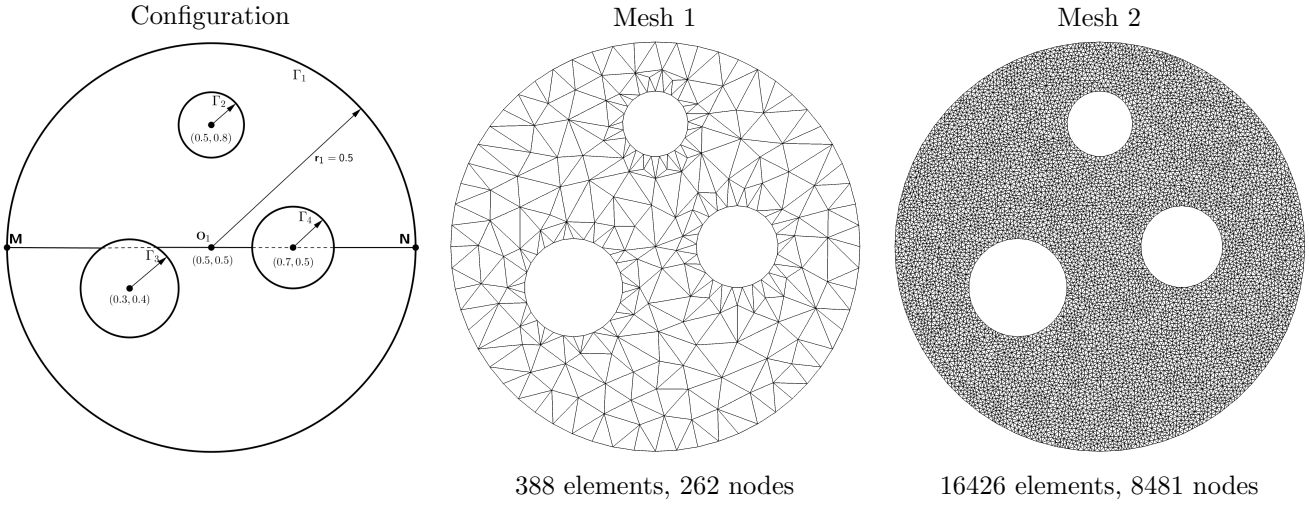

Figure 7: Configuration (m) and the considered meshes for the test example of thermal radiation in the circular enclosure.

The problem configuration and boundaries temperature are summarized in Table 4. Again in this test the governing equations are given by (6) and the diffusion coefficient is defined using the eight-frequency bands listed in Table 1. The initial temperature of the enclosure is assumed to be 1000K and a cooling process at room temperature is simulated. At the start of the simulation the heat energy will be released through the external boundary and internal holes. The ambient temperature is set to 300K on the external boundary while different temperatures are assumed on the boundaries of different holes as can be seen in Table 4. The unsymmetrical geometry and heat profile on the holes, are deliberate to test the impact on the symmetrical enrichment functions. For the PUFE solution to be accurate, the enrichment will have to capture the varying heat release rates at different parts of the domain and for the entire time span of interest. The accuracy of the PUFE method will be tested by comparing the results to those obtained using the FE method on a highly refined mesh. The two meshes considered in our simulations of this problem are shown in Figure 7. We use six enrichment functions ($Q = 6$) for the PUFE solution, comprising three Gaussian functions and three hyperbolic tangent functions. The hyperbolic enrichment is constructed with the edge parameters $\mathbf{x}_e$ as in the previous test example, however the steepness parameters are $h_1 = 0.005, h_2 = 0.25$ and $h_3 = 0.10$. The Gaussian enrichment is centred at $\mathbf{x}_c = (0.50, 0.50)^\top$ with the following steepness parameters $\gamma = \frac{18}{9}$ and $\beta = 18$. The total number of degrees of freedom used for the PUFE solution is 1572 while it is 8481 elements for the FE reference solution. The timestep is fixed to $\Delta t = 0.001$ for both FE and PUFE methods.

Figure 8 shows the distributions of the temperature in the enclosure obtained at times $t = 0.005$s, 0.01s, 0.02s. The FE reference solutions are also included in the figure at the same time instances. Despite the much coarser mesh with the PUFE method, the plots show similar heat patterns obtained using both approaches. At the first considered time instance *i.e.* $t = 0.005$s, it is clear that the solution has steep gradients on the domain boundaries. This is especially true on Γ_4 which has the lowest ambient temperature and to a lesser extent on Γ_2 and the external boundary Γ_1. The PUFE method is capable of recovering these varying heat gradients thanks to the combination of the Gaussian and hyperbolic functions that are used to enrich the numerical solution. As the time progresses the steep heat gradients are decreased which is possible to see in the snapshot presented at $t = 0.02$s in Figure 8. The drop in the heat gradient does not seem to affect the PUFE solution. Again here the PUFE method using the coarse mesh recovers the same heat patterns obtained by the reference solution.

In order to have a better insight into the accuracy, Figure 9 shows the temperature plotted at a cross-section passing through the domain and at the time instances $t = 0.005$s and 0.02s. Note that because the steepest gradient is observed at the internal boundary Γ_4 in Figure 8, we choose the cross section to pass through the centre of Γ_4. The cross section line namely (MN) is shown on the problem configuration in Figure 7. In Figure 9

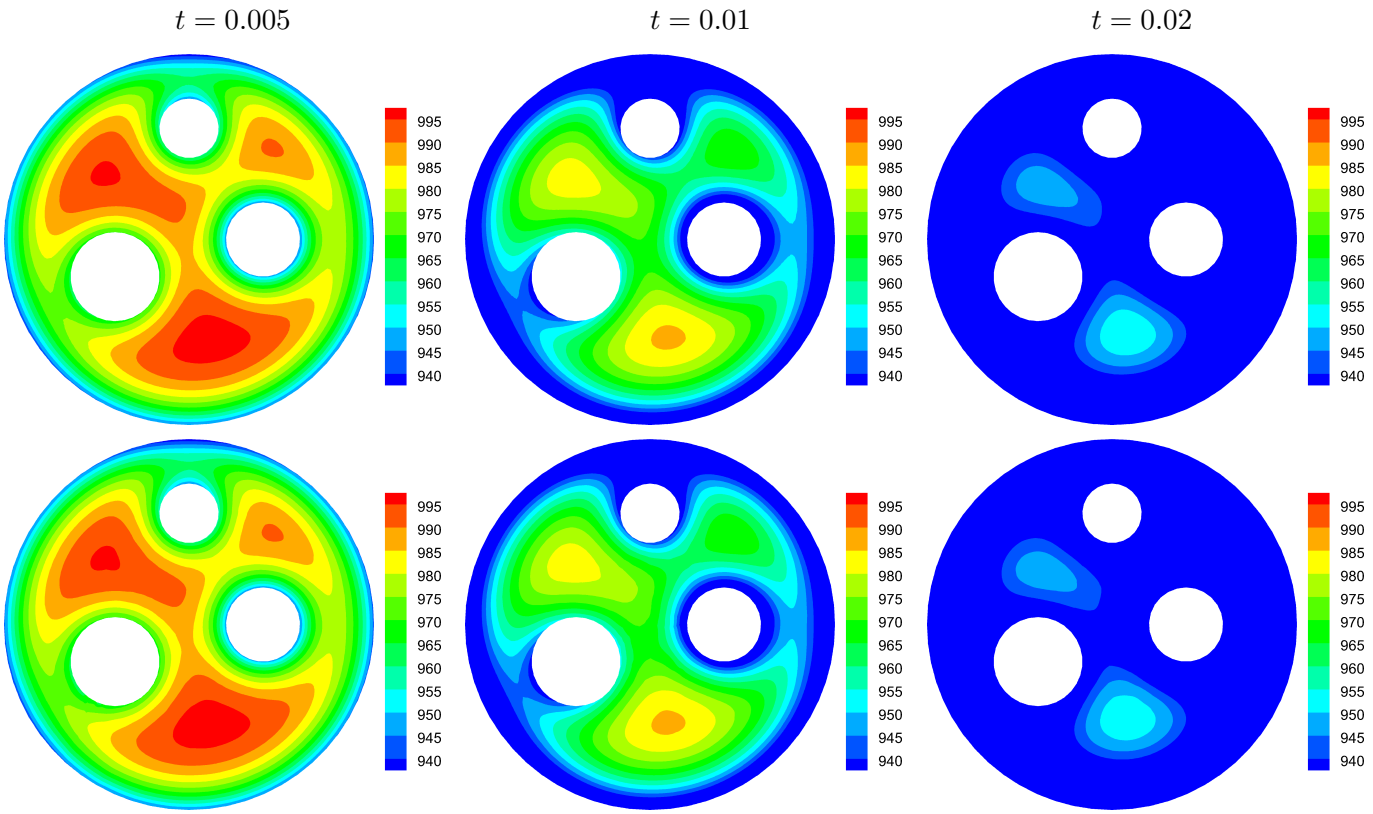

Figure 8: Temperature distributions obtained using the FE method (first row) and the PUFE method (second row) for the test example of the thermal radiation in the circular enclosure.

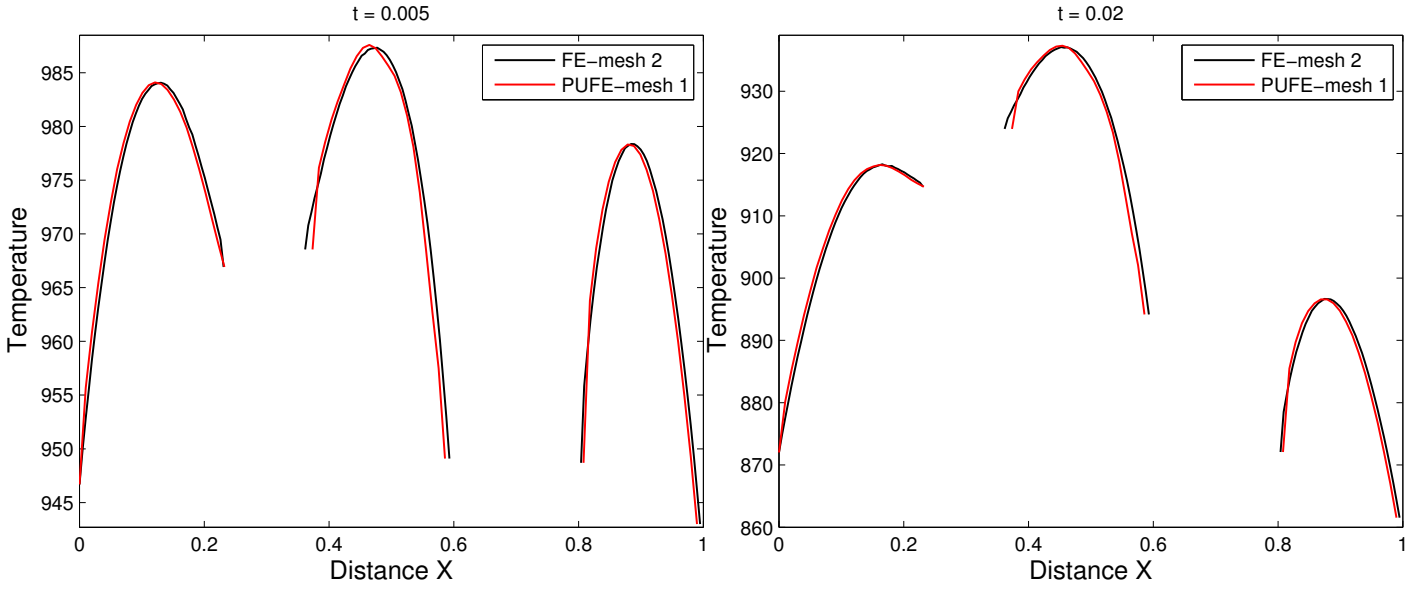

Figure 9: Cross-sections of the temperature along the horizontal centerline for the test example of the thermal radiation in the circular enclosure at $t = 0.005$s (left) and $t = 0.02$s (right).

we can observe the steep gradients associated with Γ_4 which is located in between $x = 0.6$m to 0.8m in the plots. We can also observe the steep gradient associated with the external boundary Γ_1 and that the temperature and its gradient decrease as the time progresses. The plots in this figure are consistent with the Figure 8 in showing that similar solutions are obtained with the PUFE compared to the reference solution. Furthermore, both the PUFE and the reference solutions seem to be predicting similar maximum and minimum temperatures. The results in this test case confirm our previous conclusions about the efficiency of the PUFE method and show its ability in dealing with complicated and non-symmetric geometry and/or non-symmetric heat pattern on unstructured mesh grids. Despite the large difference between the number of degrees of freedom used in the PUFE and the FE methods, both methods produced similar results.

5 Concluding remarks

In this paper we look into heat transfer in optically thick non-grey media where the thermal radiation is approximated using the Rosseland model. The full radiative heat transfer is approximated as a set of equations independent of directional coordinates and easy to be integrated in existing software packages. The optical spectrum is discretized into a finite set of frequency bands with constant absorption coefficients. The relative simplicity and the accuracy of the model for optically thick media, makes the model very popular for engineering and industrial applications. The Rosseland model significantly reduces the computational costs required for solving a problem compared to considering full radiative heat transfer. However, recovering steep boundary layers that often form in such problems requires highly refined meshes which can become very demanding computationally especially when multiple frequency bands are considered such as with non-grey media. In this work we use enriched basis functions to avoid mesh refinement. A class of Gaussian and hyperbolic tangent functions have been used as enrichment functions for the finite element space. For each frequency band a partition of unity enriched finite element method has been implemented to solve the governing equations. The enriched basis functions are used for solving the Rosseland model in a squared and circular enclosures for different optical regimes. The obtained results for thermal radiation showed that it is possible to efficiently estimate the temperature field with a computational cost significantly lower than solving the equations using the conventional finite element method. The approach is promising and can be applied to different real world applications involving the Rosseland model where predicting the thermal radiation can substantially benefit from the efficiency and accuracy of the proposed approach. Although we only consider the finite element method but the based on previous experience improvement obtained with the enriched basis functions can also be applicable to other numerical methods. Future work will concentrate on developing adaptive enrichments based on an error estimator for each frequency band in the optical spectrum and extension of these approaches to thermal radiation in non-grey three-dimensional enclosures using high-order Legendre polynomials.

References

[1] R. Borker, C. Farhat, and R. Tezaur. A discontinuous Galerkin method with Lagrange multipliers for spatially-dependent advection-diffusion problems. *Comput. Methods. Appl. Mech. Eng.*, 327:93–117, 2017.

[2] S. Chandrasekhar. *Radiative Transfer*. Oxford University Press, London, 1950.

[3] R.M.S. da Gama, E.D. Corrêa, and M.L. Martins-Costa. An upper bound for the steady-state temperature for a class of heat conduction problems wherein the thermal conductivity is temperature dependent. *Int. J. Eng. Sci.*, 69:77–83, 2013.

[4] P.S. Datti, K.V. Prasad, M.S. Abel, and A. Joshi. MHD visco-elastic fluid flow over a non-isothermal stretching sheet. *Int. J. Eng. Sci.*, 42(8-9):935–946, 2004.

[5] B. Dietrich, T. Fischedick, S. Heissler, P.G. Weidler, C. Wöll, and M. Kind. Optical parameters for characterization of thermal radiation in ceramic sponges-experimental results and correlation. *Int. J. Heat Mass Transf.*, 79:655–665, 2014.

[6] G.C. Diwan and M.S. Mohamed. Pollution studies for high order isogeometric analysis and finite element for acoustic problems. *Computer Methods in Applied Mechanics and Engineering*, 350:701–718, 2019.

[7] G.C. Diwan, M.S. Mohamed, M. Seaid, J. Trevelyan, and O. Laghrouche. Mixed enrichment for the finite element method in heterogeneous media. *Int. J. Numer. Methods Eng.*, 101(1):54–78, 2015.

[8] S. Duerigen and E. Fridman. The simplified P3 approach on a trigonal geometry of the nodal reactor code DYN3D. *Kerntechnik*, 77(4):226–229, 2012.

[9] C. Farhat, I. Harari, and U. Hetmanuk. A discontinuous Galerkin method with Lagrange multipliers for the solution of Helmholtz problems in the midfrequency regime. *Comput. Methods. Appl. Mech. Eng.*, 192:1389–1419, 2003.

[10] C. Farhat, I. Kalashnikova, and R. Tezaur. A higher-order discontinuous enrichment method for the solution of high Péclet advection–diffusion problems on unstructured meshes. *Int. J. Numer. Methods Eng.*, 81(5):604–636, 2010.

[11] R.C. Moro Filho and W. Malalasekera. An analysis of thermal radiation in porous media under local thermal non-equilibrium. *Transp. Porous Media*, 132:683–705, 2020.

[12] M. Frank, M. Seaid, J. Janicka, A. Klar, R. Pinnau, and G. Thömmes. A comparison of approximate models for radiation in gas turbines. *Int. J. Prog. Comput. Fluid. Dy.*, 3:191–197, 2004.

[13] C.J. Gittelson and R. Hiptmair. Dispersion analysis of plane wave discontinuous Galerkin methods. *Int. J. Numer. Methods Eng.*, 98(5):313–323, 2014.

[14] ITWM. *Fraunhofer-Institut für Techno- und Wirtschaftsmathematik, Kaiserslautern, Germany.* http://www.itwm.de.

[15] I. Kalashnikova, R. Tezaur, and C. Farhat. A discontinuous enrichment method for variable-coefficient advection–diffusion at high Péclet number. *Int. J. Numer. Methods Eng.*, 87(1-5):309–335, 2011.

[16] A. Klar, J. Lang, and M. Seaid. Adaptive solutions of SP_N-approximations to radiative heat transfer in glass. *Int. J. Therm. Sci.*, 44:1013–1023, 2005.

[17] R. Koch, W. Krebs, S. Wittig, and R. Viskanta. Discrete ordinate quadrature schemes for multidimensional radiative transfer. *J. Quant. Spectrosc. Radiat. Transf.*, 53:353–372, 1995.

[18] S. Kuske. *Modelling of radiative heat transfer in sooting flames.* Technical University Graz, 1999.

[19] O. Laghrouche and P. Bettess. Short wave modelling using special finite elements. *J. Comput. Acoust.*, 8(01):189–210, 2000.

[20] E. Larsen, G. Thömmes, A. Klar, M. Seaid, and T. Götz. Simplified P_N approximations to the equations of radiative heat transfer and applications. *J. Comput. Phys.*, 183:652–675, 2002.

[21] B. Le Corre, A. Collin, L. Soudre-Bau, Y. Meshaka, and G. Jeandel. Glass sagging simulation with improved calculation of radiative heat transfer by the optimized reciprocity monte carlo method. *Int. J. Heat Mass Transf.*, 70:215–223, 2014.

[22] H. Li and C.A. Duarte. A two-scale generalized finite element method for parallel simulations of spot welds in large structures. *Comput. Methods. Appl. Mech. Eng.*, 337:28–65, 2018.

[23] T. Luostari, T. Huttunen, and P. Monk. The ultra weak variational formulation using bessel basis functions. *Commun. Comput. Phys.*, 11(2):400, 2012.

[24] M. Malek, N. Izem, M.S. Mohamed, and M. Seaid. A three-dimensional enriched finite element method for nonlinear transient heat transfer in functionally graded materials. *Int. J. Heat Mass Transf.*, 155:119804, 2020.

[25] M. Malek, N. Izem, M.S. Mohamed, M. Seaid, and O. Laghrouche. A partition of unity finite element method for three-dimensional transient diffusion problems with sharp gradients. *J. Comput. Phys.*, 396:702–717, 2019.

[26] M. Malek, N. Izem, M. Seaid, M.S. Mohamed, and M. Wakrim. A partition of unity finite element method for nonlinear transient diffusion problems in heterogeneous materials. *Comput. Appl. Math.*, 38:31, 2019.

[27] S. G. Martyushev and M.A. Sheremet. Characteristics of rosseland and P1 approximations in modeling nonstationary conditions of convection-radiation heat transfer in an enclosure with a local energy source. *J. Eng. Phys. Thermophys.*, 21:111–118, 2012.

[28] J.M. Melenk and I. Babuška. The partition of unity finite element method: Basic theory and applications. *Comput. Methods. Appl. Mech. Eng.*, 139:289–314, 1996.

[29] D. Mihalas and B.S. Mihalas. *Foundations of Radiation Hydrodynamics*. Oxford University Press, New York, 1983.

[30] M.F. Modest. *Radiative Heat Transfer*. McGraw-Hill, 1993.

[31] M.S. Mohamed, M. Seaid, and A. Bouhamidi. Iterative solvers for generalized finite element solution of boundary-value problems. *Numerical Linear Algebra with Applications*, 25(6):e2205, 2018.

[32] M.S. Mohamed, M. Seaid, J. Trevelyan, and O. Laghrouche. A partition of unity fem for time-dependent diffusion problems using multiple enrichment functions. *Int. J. Numer. Methods Eng.*, 93:245–265, 2013.

[33] M.S. Mohamed, M. Seaid, J. Trevelyan, and O. Laghrouche. Time-independent hybrid enrichment for finite element solution of transient conduction-radiation in diffusive grey media. *J. Comput. Phys.*, 251:81–101, 2013.

[34] M.S. Mohamed, M. Seaid, J. Trevelyan, and O. Laghrouche. An enriched finite element model with q-refinement for radiative boundary layers in glass cooling. *J. Comput. Phys.*, 258:718–737, 2014.

[35] E.A. Munts, S.J. Hulsho, and R. de Borst. The partition-of-unity method for linear diffusion and convection problems: Accuracy, stabilization and multiscale interpretation. *Int. J. Numer. Methods Eng.*, 43:199–213, 2003.

[36] M. Nawaz. Role of hybrid nanoparticles in thermal performance of sutterby fluid, the ethylene glycol. *Physica A*, 537:122447, 2019.

[37] M. Nawaz, I. H. Qureshi, and A. Shahzad. Thermal performance of partially ionized eyring–powell liquid: a theoretical approach. *Phys. Scr.*, 94:35222, 2019.

[38] M. Nawaz, S. Rafiq, I. H. Qureshi, and S. Saleem. Combined effects of partial slip and variable diffusion coefficient on mass and heat transfer subjected to chemical reaction. *Phys. Scr.*, 95:125209, 2020.

[39] P. O'Hara, C.A. Duarte, and T. Eason. Generalized finite element analysis of three-dimensional heat transfer problems exhibiting sharp thermal gradients. *Comput. Methods. Appl. Mech. Eng.*, 198:1857–1871, 2009.

[40] P. O'Hara, C.A. Duarte, and T. Eason. Transient analysis of sharp thermal gradients using coarse finite element meshes. *Comput. Methods. Appl. Mech. Eng.*, 200:812–829, 2011.

[41] E. Perrey-Debain, J. Trevelyan, and P. Bettess. Wave boundary elements: a theoretical overview presenting applications in scattering of short waves. *Eng. Anal. Bound. Elem.*, 28:131–141, 2004.

[42] S. Rosseland. *Theoretical Astrophysics. Atomic Theory and the Analysis of Stellar Atmospheres and Envelopes*. Clarendon Press, Oxford, 11936.

[43] J.C. Sanders. *Nonlinear Transient Conduction Heat Transfer Using a Discontinuous Galerkin Hierarchical Finite Element Method*. George Washington University, 2004.

[44] M. Seaid. Multigrid newton-krylov method for radiation in diffusive semitransparent media. *J. Comput. Appl. Math.*, 203:498–515, 2007.

[45] M. Seaid, A. Klar, and R. Pinnau. Numerical solvers for radiation and conduction in high temperature gas flows. *Flow, turbulence and combustion*, 75(1-4):173–190, 2005.

[46] B. van der Linden. *Radiative heat transfer in glass*. Technische Universiteit Eindhoven, 2002.

[47] F.P. van der Meer, R. Al-Khoury, and L.J. Sluys. Time-dependent shape functions for modeling highly transient geothermal systems. *Int. J. Numer. Methods Eng.*, 77:240–260, 2009.

[48] R. Viskanta and E.E. Anderson. Heat transfer in semitransparent solids. *Adv. Heat Transf.*, 11:318–441, 1975.

[49] F. Wang, J. Tan, S. Yong, H. Tan, and S. Chu. Thermal performance analyses of porous media solar receiver with different irradiative transfer models. *Int. J. Heat Mass Transf.*, 78:7–16, 2014.